A Stochastic Model of Sea-Surface Roughness. II

Michael S. Longuet-Higgins

Proceedings: Mathematical and Physical Sciences, Vol. 435, No. 1894 (Nov. 8, 1991), 405-422.

Stable URL:
http://links.jstor.org/sici?sici=0962-8444%2819911108%29435%3A1894%3C405%3AASMOSR%3E2.0.CO%3B2-G

Proceedings: Mathematical and Physical Sciences is currently published by The Royal Society.

A stochastic model of sea-surface roughness. II

By Michael S. Longuet-Higgins

Institute for Nonlinear Science, University of California San Diego, La Jolla, California 92093-0402, U.S.A.

A two-scale model of a wind-ruffled surface is developed which includes (1) modulation of the short waves by orbital straining in the long waves, (2) dissipation of short-wave energy by breaking, and (3) regeneration of the short-wave energy by the wind. For simplicity the long waves are at first assumed to be uniform. It is shown that the character of the surface is governed by the parameter $\Omega = \beta/(\sigma\gamma KA)$, where β is the proportional rate of short-wave growth due to the wind, σ, K and A are the long-wave frequency wavenumber and amplitude, and $\gamma = 2.08$. When $\Omega < 1$ the short waves break over only part of the long-wave surface. When $\Omega \geqslant 1$ they break everywhere.

The mean-square steepness $\overline{s^2}$ of the short waves is an increasing function of β/σ, but a decreasing function of the long-wave steepness AK. The phase angle between $\overline{s^2}$ and the long-wave elevation η is an increasing function of Ω. The correlation between $\overline{s^2}$ and η is largest when $\Omega \ll 1$, but tends to 0 as $\Omega \to 1$.

The simple model is extended to the case when the long-wave amplitude A has a Rayleigh probability density. To take account of the 'sheltering' effect of high waves we compute the case when any two successive waves have a bivariate Rayleigh density.

The application of the model to laboratory and field data is discussed.

1. Introduction

The hydrodynamical interaction of short waves with longer waves on the sea surface has important consequences both for air–sea transfer processes and for the imaging of the ocean surface by certain types of remote sensors which depend upon Bragg scattering from the shorter waves. References are given in Longuet-Higgins (1987; referred to as part I). In that paper, a model of the short-waves dynamics was presented which included the following features: (*a*) modulation of the short-wave steepness by orbital straining in the longer waves; (*b*) dissipation of short-wave energy by breaking, particularly near crests of the longer waves; (*c*) regeneration of the short-wave energy by the wind; (*d*) a random distribution of long-wave amplitude.

Particular attention was paid to the behaviour of the short waves at the long-wave crests, and it was shown how an integral equation could be formulated for the probability density $p(s\,|\,A)$ of the short-wave steepness s at the crest of a longer wave of given amplitude A. In part I the author looked forward to a study of the characteristics of the short waves over the whole profile of the longer waves. From these one could obtain several parameters of interest such as the mean-square short-wave steepness $\overline{s^2}$ over the whole wave surface, and the phase and amplitude modulation of s^2 relative to the long waves.

Proc. R. Soc. Lond. A (1991), **435**, 405–422
Printed in Great Britain

The present paper gives the results of this study. To present and interpret them we first describe a simplified model which includes the elements (*a*), (*b*) and (*c*) above but omits, for the time being, the random element (*d*). This simplified model is described in §§2 and 3 below, and its consequences are discussed in §§4 and 5.

Randomness is then introduced in two stages. A partially random model, in which the long-wave amplitude has a Rayleigh density but the wave height is locally uniform (a narrow-band spectrum) is studied in §6. Then in §7 we re-introduce the full bivariate Rayleigh distribution for the long wave amplitude, and present the numerical results. In §§8 and 9 we make comparisons with laboratory and field data. A discussion follows in §10.

2. Physical assumptions

We assume that the surface-slope spectrum may be effectively divided into two parts as follows. First, a narrow, low-frequency part, to be called the 'long waves'. A representative amplitude and wavenumber for these being denoted by A and K, the corresponding surface elevation is given by

$$\eta = A\cos\theta, \quad \theta = \sigma t + Kx + \epsilon, \tag{2.1}$$

where x is a horizontal coordinate, t is the time. A and ϵ are functions of x and t which vary slowly compared with the phase θ. If σ and K are both positive, the waves move to the left, as in figure 1.

Superposed on the long waves we assume a much shorter, wind-generated, 'surface roughness' with local mean-square slope s^2. Following Plant (1982) we assume that, below saturation, s grows exponentially with time:

$$s \propto \mathrm{e}^{\beta t}, \tag{2.2}$$

say, where the growth-rate β depends upon both the wind-speed W and on the frequency of the short waves. Here we shall take β to correspond to the mean short-wave frequency σ', say. Note that the empirical law (2.2) already takes some account of the nonlinear interactions among the short waves themselves. However, the short-wave steepness is assumed to be limited by breaking at a critical steepness s_0, say. For the reasons given in part I we choose

$$s_0 = 0.22, \quad s_0^2 = 0.0484, \tag{2.3}$$

which is consistent with the limits on s found by Plant (1982).

In the absence of wind, the relative steepening of the short waves due to the orbital motion in the long waves has been shown to be given by

$$s \propto \mathrm{e}^{\gamma K \eta} \tag{2.4}$$

approximately, where $\gamma = 2.08$ (see Longuet-Higgins 1986). Hence (when the short waves are not limited by breaking) we combine (2.2) and (2.4) to give

$$s \sim \mathrm{e}^{\beta t + \gamma K \eta}, \tag{2.5}$$

η being given by (2.1). Thus

$$\frac{\partial s}{\partial t} = \begin{cases} (\beta + \gamma K\, \partial\eta/\partial t)\, s, & s < s_0 \\ 0, & s = s_0 \end{cases}. \tag{2.6}$$

The case $s = s_0$ corresponds to the parts of the surface where the short-wave steepness is limited by breaking.

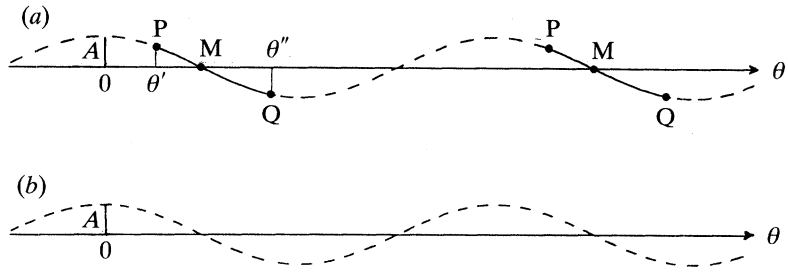

Figure 1. Time-history of short waves on a uniform train of long waves. The broken line indicates intervals where the short waves are breaking. (*a*) $\Omega < 1$, (*b*) $\Omega \geqslant 1$.

Lastly, we assume that the short waves have a negligible short-term influence on the long waves, and that the system is in a statistically steady state. Thus there is an overall balance between the input of short-wave energy by the wind and the loss of short-wave energy by breaking at the limiting root-mean square (r.m.s.) steepness s_0.

We shall now explore the properties of this model.

3. A uniform train of long waves

Suppose first that the wave amplitude A is uniform and the phase ϵ is zero (figure 1). Since the waves are statistically steady, and short-wave energy is being supplied by the wind, the short waves must be breaking somewhere. Therefore they are certainly breaking at the long-wave crests, where the short-wave steepening due to the long-wave orbital motion is at its greatest. Let us follow a group of short waves as it is carried by the orbital motion of the long waves. We assume that its group-velocity is small compared to $A\sigma$. As the long waves move forward beneath the short waves there may come a point P, on the windward face of the long waves, where the straining of the short waves overcomes the wind input, i.e. $\partial s/\partial t$ falls below zero. From equation (2.6) this point is given by $\theta = \theta'$, where

$$\beta - \gamma KA\sigma \sin\theta' = 0. \tag{3.1}$$

We have then

$$\sin\theta' = \Omega, \tag{3.2}$$

where we have written

$$\Omega = (\beta/\sigma)/\gamma KA. \tag{3.3}$$

For P to be real we must have $\Omega \leqslant 1$. When $\Omega < 1$, P lies above the mean level M, at which the orbital straining is a maximum. Thus $0 < \theta' < \frac{1}{2}\pi$.

Between P and Q the waves are not breaking, so by equation (2.5) we must have

$$s = s_0 \exp[\beta(t-t') + \gamma K(\eta - \eta')], \tag{3.4}$$

where t' and η' denote the values of t and η when $\theta = \theta'$. In figure 1, θ'' denotes the point where s again equals s_0. This will be when the exponent in (3.4) vanishes. For fixed x we have $\sigma(t-t') = \theta - \theta'$. So

$$(\beta/\sigma)(\theta'' - \theta') + \gamma KA(\cos\theta'' - \cos\theta') = 0. \tag{3.5}$$

From (3.5) it follows that

$$(\cos\theta'' - \cos\theta')/(\theta'' - \theta') = -\Omega, \tag{3.6}$$

where Ω is the same combination of constants as in (3.3).

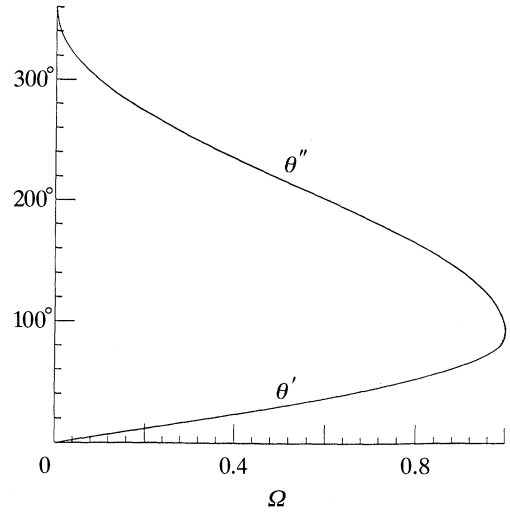

Figure 2. The critical phase-angles θ' and θ'' as a function of $\Omega = \beta/\gamma\sigma AK$.

Suppose Ω to be given. If $\theta > 1$ then equation (3.2) has no solution. Physically this means that the wind is blowing so strongly that the short waves are everywhere breaking. If on the other hand $\Omega \leqslant 1$ then equation (3.3) may be solved for θ', and from (3.7) we can then find θ''.

The results are shown in figure 2, where θ' and θ'' are plotted against Ω throughout the range $0 < \Omega \leqslant 1$. For example when $\Omega \ll 1$ (a relatively light wind) then θ' is small and θ'' approaches 2π. Thus P and Q approach the crest from either side. This means that short-wave breaking is confined to the neighbourhood of the long-wave crests.

On the other hand when Ω approaches 1, then both θ' and θ'' approach 90°, so P and Q approach the point M ($\theta = \frac{1}{2}\pi$). Physically, the short waves are breaking almost everywhere, and only near the mean water level do we have $s < s_0$. By expansion of the left-hand sides of (3.2) and (3.7) in powers of the small angles

$$\alpha' = \tfrac{1}{2}\pi - \theta', \quad \alpha'' = \theta'' - \tfrac{1}{2}\pi \tag{3.8}$$

we find

$$\alpha' = (1-\Omega^2)^{\frac{1}{2}}, \quad \alpha'' = 2(1-\Omega^2)^{\frac{1}{2}}. \tag{3.9}$$

In other words, Q is twice as far from M as is P.

4. Statistical properties

For comparison with observation, three numerical quantities are specially useful, namely the mean-square slope

$$\overline{s^2} = \frac{1}{2\pi}\int_0^{2\pi} s^2(\theta)\,\mathrm{d}\theta, \tag{4.1}$$

the correlation function

$$C(\phi) = \overline{s^2(\theta)\,\eta(\theta-\phi)} = \frac{1}{2\pi}\int_0^{2\pi} s^2(\theta)\,\eta(\theta-\phi)\,\mathrm{d}\phi \tag{4.2}$$

and the correlation coefficient

$$C^*(\phi) = C(\phi)/(\overline{s^4\eta^2})^{\frac{1}{2}}, \tag{4.3}$$

where a bar denotes an average with respect to x or t. Of particular interest are the maximum value $C_{\max}$ of $C(\phi)$ and the phase-angle ϕ_m at which the maximum is attained.

Now in the simple model of §3 we have

$$s^2 = s_0^2[1+F(\theta)], \tag{4.4}$$

where

$$F(\theta) = \begin{cases} -1+\exp\left[(2\beta/\sigma)(\theta-\theta')+2\gamma AK(\cos\theta-\cos\theta')\right] & \text{when } \theta' < \theta < \theta'', \\ 0, & \text{otherwise.} \end{cases} \tag{4.5}$$

Hence

$$\overline{s^2} = s_0^2\left[1+\frac{1}{2\pi}\int_{\theta'}^{\theta''} F(\theta)\,\mathrm{d}\theta\right] \tag{4.6}$$

and

$$\overline{s^4} = s_0^4\left[1+\frac{1}{2\pi}\int_{\theta'}^{\theta''} (2F+F^2)\,\mathrm{d}\theta\right]. \tag{4.7}$$

Further, in (4.2) we can substitute for η from equation (2.1) to obtain

$$C(\phi) = s_0^2 A(X\cos\phi + Y\sin\phi)/2\pi, \tag{4.8}$$

where

$$X = \frac{1}{2\pi}\int_{\theta'}^{\theta''} F(\theta)\cos\theta\,\mathrm{d}\theta, \quad Y = \frac{1}{2\pi}\int_{\theta'}^{\theta''} F(\theta)\sin\theta\,\mathrm{d}\theta. \tag{4.9}$$

Equation (4.8) shows that $C(\theta)$ takes its maximum value when $\phi = \phi_0$, where

$$\cos\phi_0 = X/(X^2+Y^2)^{\frac{1}{2}}, \quad \sin\phi_0 = Y/(X^2+Y^2)^{\frac{1}{2}} \tag{4.10}$$

and that

$$C_{\max} = s_0^2 A(X^2+Y^2)^{\frac{1}{2}}. \tag{4.11}$$

Hence also

$$C^*_{\max} = (X^2+Y^2)^{\frac{1}{2}}/2^{\frac{1}{2}}Z \tag{4.12}$$

and

$$C^*(0) = X/2^{\frac{1}{2}}Z, \tag{4.13}$$

where

$$Z^2 = 1+\frac{1}{2\pi}\int_{\theta'}^{\theta''} (2F+F^2)\,\mathrm{d}\theta. \tag{4.14}$$

We consider now some limiting values. When Ω approaches 1 from below, then $(\theta''-\theta')\to 0$ and from equation (4.6) we have

$$\overline{s^2}/s_0^2 \to 1. \tag{4.15}$$

Also from (4.9) and (4.10), we see that $X\to 0$ and $Y\to -0$ (since $F \leqslant 0$) and $Y/X\to 0$, hence

$$\phi_0 \to -90°, \tag{4.16}$$

while from (4.14), $R\to(2\pi)^{\frac{1}{2}}$, hence

$$C^*_{\max}\to 0, \quad C^*(0)\to 0. \tag{4.17}$$

Note that in physical space (θ decreasing) s^2 leads η by 90°. This is because s^2 has a small dip in the non-breaking region on the rear slope of the wave, which leads the minimum of η (the wave trough) by 90°.

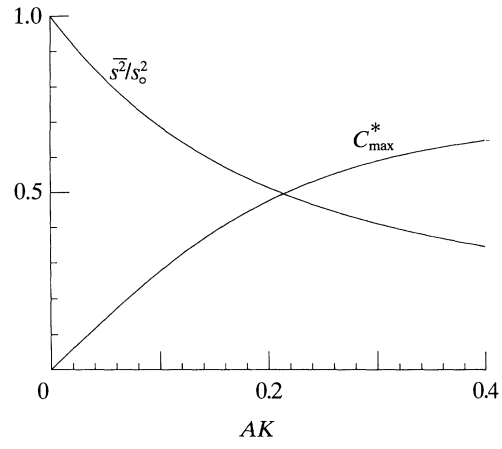

Figure 3. The relative mean-square slope $\overline{s^2}/s_0^2$ and correlation coefficient $C^*_{\max}$ as functions of AK in the limiting case $\Omega \to 0$.

On the other hand when $\Omega \ll 1$ and so the wind-generation factor is relatively small, breaking will occur only close to the wave crests. Hence $\theta' \to 0$ and $\theta'' \to 2\pi$ and from equation (3.5) we have in the limit

$$s^2/s_0^2 = \exp\left[2\gamma AK(\cos\theta - 1)\right] \tag{4.18}$$

throughout $0 < \theta < 2\pi$. From (4.1) we find then

$$\overline{s^2}/s_0^2 = \mathrm{e}^{-z} I_0(z), \tag{4.19}$$

where

$$z = 2\gamma AK \tag{4.20}$$

and I_0 denotes the modified Bessel function of order zero. Similarly from equations (4.9) we have

$$X = \mathrm{e}^{-z} I_1(z), \quad Y = 0 \tag{4.21}$$

so that the phase ϕ_0 vanishes. Also from (4.14)

$$Z^2 = \mathrm{e}^{-2z} I_0(2z). \tag{4.22}$$

Hence by (4.12) and (4.13)

$$C^*_{\max} = C^*(0) = 2^{\frac{1}{2}} I_1(z)/[I_0(2z)]^{\frac{1}{2}}. \tag{4.23}$$

The above expressions for $\overline{s^2}/s_0^2$ and $C^*_{\max}$ are plotted as functions of $AK = z/2\gamma$ in figure 3.

5. Numerical results

For general values of AK and β/σ the integrals in equation (4.6), (4.7) and (4.9) are easy to compute, and in figure 4*a–d* we have plotted contours of $\overline{s^2}/s_0^2$, ϕ_0, $\hat{C}_{\max}$ and $\hat{C}(0)$ respectively, as functions of AK and β/σ. From (3.3) it is clear that the loci $\Omega = $ const. are straight lines at a 45° angle. In particular the locus $\Omega = 1$ corresponds to the straight line on the lower right-hand corner of each figure.

It will be seen that each of the quantities $\overline{s^2}/s_0^2$, C^*, ϕ_0 and $C^*(0)$ varies monotonically with AK or with β/σ. In particular, as the long-wave steepness is held constant but the wind generation factor β/σ is increased, so $\overline{s^2}/s_0^2$ increases, as one

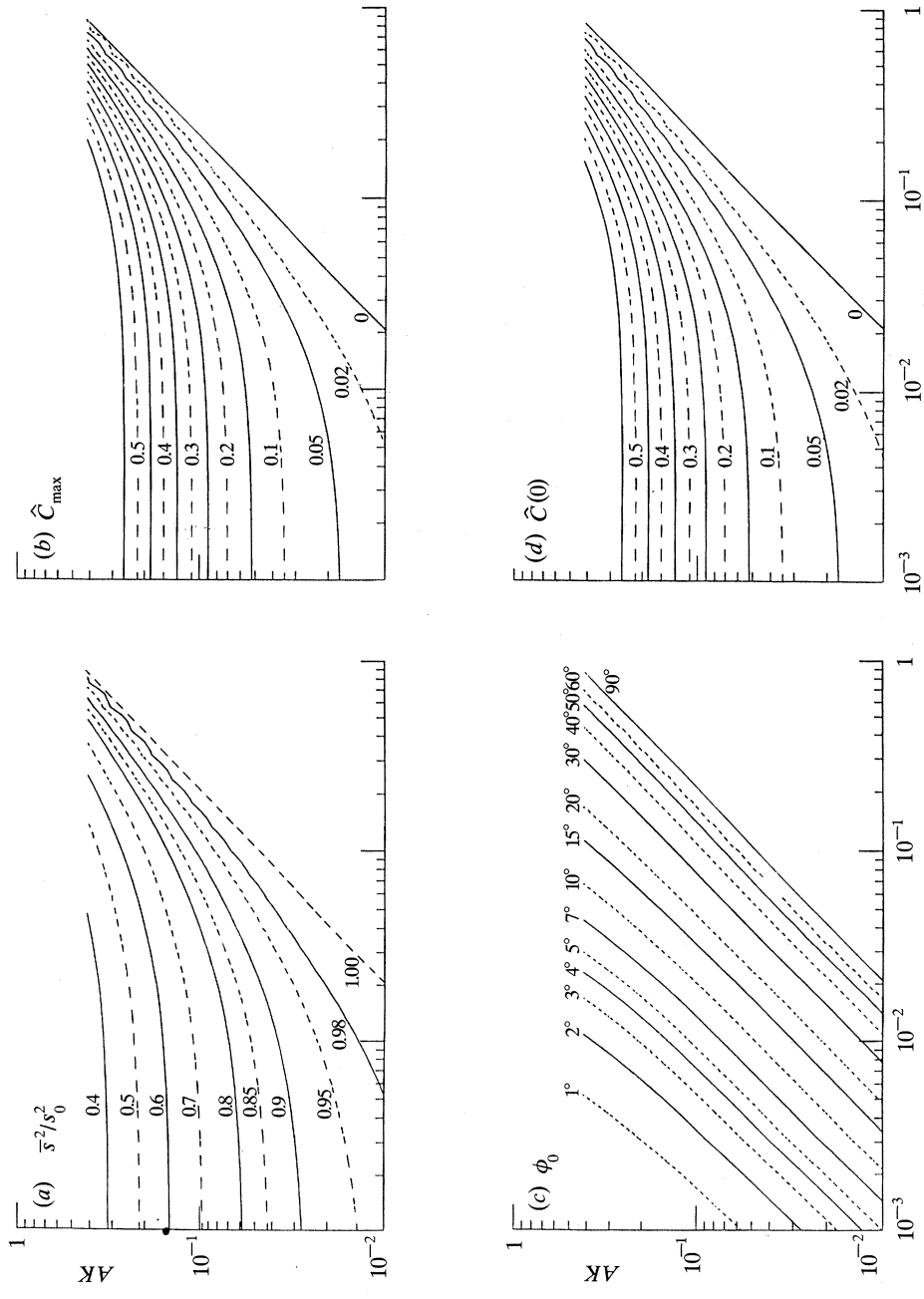

Figure 4. Statistical parameters for short waves on a uniform train of long waves. (*a*) $\overline{s^2}/s_0^2$, (*b*) $\hat{C}_{\max}$, (*c*) ϕ_0, (*d*) $\hat{C}(0)$.

might expect. More interestingly, for constant wind, $\overline{s^2}/s_0^2$ is a decreasing function of the long-wave steepness AK. This is due to the increased amount of short-wave stretching, away from the long-wave crests.

As $\beta/\sigma \to 0$, the limiting values of $\overline{s^2}/s_0^2$ and $C_{\max}$ are given by (4.19) and (4.23) respectively. Since for small values of z

$$I_0(z) = 1+\tfrac{1}{4}z^2, \quad I_1(z) = \tfrac{1}{2}z(1+\tfrac{1}{8}z^2) \tag{5.1}$$

we have
$$\overline{s^2}/s_0^2 = 1-z+\tfrac{3}{4}z^2 \tag{5.2}$$

and
$$C^*_{\max} = (z/2^{\frac{1}{2}})(1-\tfrac{3}{8}z^2), \tag{5.3}$$

where
$$z = 2\gamma AK. \tag{5.4}$$

In general, the phase ϕ_0 appears from figure 4*c* to be a function of Ω alone. At least for small values of AK and β/σ this may be understood as follows. From (3.2) and (3.7),

$$\theta' = \Omega, \quad \text{and} \quad \theta'' = 2\pi-(4\pi\Omega)^{\frac{1}{2}} \tag{5.5}$$

to lowest order in Ω, and so from (4.5)

$$F(\theta) = 2(\beta/\sigma)(\theta-\theta')+2\gamma AK(\cos\theta-\cos\theta') \tag{5.6}$$

On substituting for $F(\theta)$ in (4.9) we find, to lowest order,

$$X = 2\pi\gamma AK, \quad Y = -4\pi\beta/\sigma, \tag{5.7}$$

hence
$$\tan\phi_0 = (2\beta/\sigma)/\gamma AK = 2\Omega. \tag{5.8}$$

In this limiting case, the mean-square steepness s^2 still leads the surface elevation η in physical space, but this is due mainly to the exponential growth factor β from the wind input. Also since $(2\pi-\theta'')$ is greater than θ' (see figure 2) the region of breaking extends further down the forward face of the wave than down the next rear face.

In each of figure 4*a–d*, the theoretical values to the right of the line $\Omega = 1$ are constant.

6. Random long waves: the Rayleigh distribution

So far we have assumed the height of the long waves to be uniform. In a real sea state having a fairly narrow-band spectrum, the amplitude A of the dominant waves has a probability density that is closely Rayleigh (see Longuet-Higgins 1980). Thus

$$p(A) = (A/A_0^2)\,\mathrm{e}^{-A^2/2A_0^2}, \tag{6.1}$$

where A_0 is a constant related to the mean-square wave amplitude $\langle A^2\rangle$ by

$$\langle A^2\rangle = 2A_0^2. \tag{6.2}$$

With the aid of (6.1) we may generate the results of §2 to the case when the amplitude A is not quite uniform but instead varies slowly, the groups of waves being relatively long.

Since σ is assumed constant, the parameter β/σ will be fixed, for a given wind-speed. The effect of distributing the amplitude A will be to average the values of $\overline{s^2}$ in figure 3, for example, by means of the probability density $p(A)$. So we may extend the definitions of §4 by calculating

$$\langle\overline{s^2}\rangle = \left\langle \frac{1}{2\pi}\int s^2(0)\,\mathrm{d}\theta \right\rangle \tag{6.3}$$

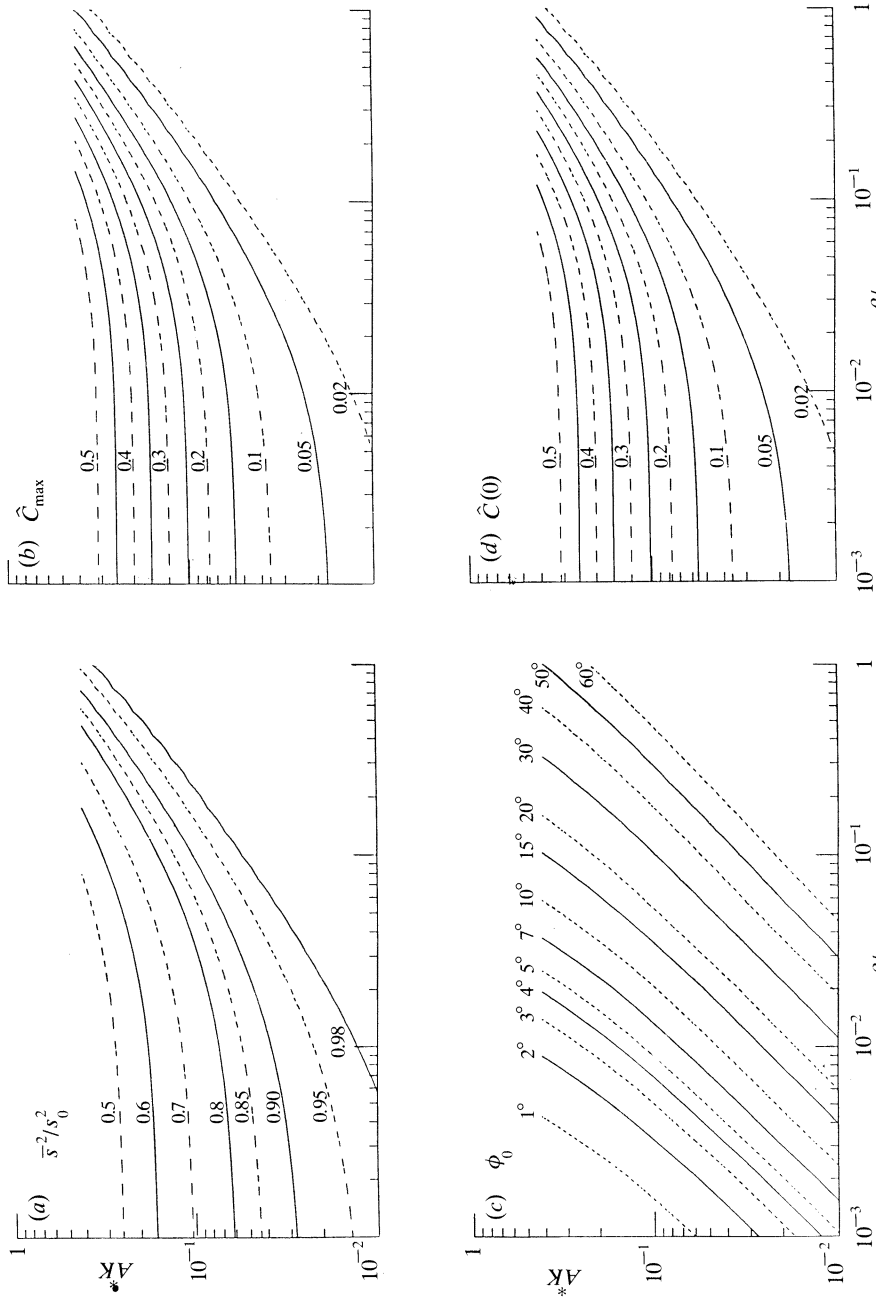

Figure 5. As figure 4, but for a Rayleigh-distributed long-wave amplitude. $\kappa = 1$.

in which $\langle\ \rangle$ denotes the statistical average. Similarly we may define the average quantities $\langle C^*(\phi)\rangle$, $\langle\overline{s^4}\rangle$ and $\langle\overline{\eta^2}\rangle 0$, and finally, as in equation (4.3),

$$C(\phi) = \langle C^*(\phi)\rangle/[\langle\overline{s^4}\rangle\langle\eta^4\rangle]^{\frac{1}{2}}. \tag{6.4}$$

The angle ϕ, is defined as previously, as the angle for which $C(\phi)$ takes its maximum value $C_{\max}$.

The results are shown in figure 5*a–d* as functions of A^*K and β/σ, where

$$A^* = \langle A\rangle = (\tfrac{1}{2}\pi)^{\frac{1}{2}}A_0 \tag{6.5}$$

denotes the average long wave amplitude. Figure 5*a* showing $\langle\overline{s^2}\rangle/s_0^2$, may be compared with figure 4*a*. The form of the contours is very similar, except that the diagonal contour in figure 4*a* corresponding to $\Omega = 1$ is now smoothed over.

Similarly figure 5*b* showing ϕ corresponds closely to figure 4*b*, and figure 5*c* showing $C_{\max}$ corresponds closely to figure 4*c*. In both figures 4*a* and 5*a*, for example, the contours of constant ϕ_0 have a slope of nearly unity, indicating that ϕ_0 is a function of $A^*K/(\sigma/B)$ very nearly.

7. The bivariate Rayleigh distribution

Even in the randomized model of §6, the short waves always break at long-wave crests. In actual sea states, however, a high wave may often be followed by a significantly lower wave. Because of orbital stretching, the short waves may not break at the crests of the second waves, even if they break on the first. Similarly a non-breaking wave may be followed either by a breaking or by a non-breaking wave.

A general stochastic model which takes into account all such possibilities was developed in part I. There, the joint probability density of two successive wave amplitudes A_1 and A_2 was assumed to be given by the bivariate Rayleigh density:

$$p(A_1, A_2) = \frac{A_1 A_2}{(1-\kappa^2)A_0^4}\exp\left[-(A_1^2+A_1^2)/2(1-\kappa^2)A_0^2\right] I_0\left(\frac{\kappa A_1 A_2}{(1-\kappa^2)A_0^2}\right). \tag{7.1}$$

Here A_0^2 denotes half the mean-square amplitude as before, I_0 is the modified Bessel function of order zero and κ is a 'groupiness' parameter, related explicitly to the spectral density of η. For narrow spectra it can be shown that $\kappa^2 = 1-(2\pi\nu)^2$, where ν is the spectral band-width. For very narrow spectra we have $\kappa \approx 1$. This is the limiting case corresponding to the model of §6. On the other hand for very broad spectra $\kappa \to 0$ and then A_1 and A_2 are statistically independent:

$$p(A_1, A_2) = p(A_1)\,p(A_2), \tag{7.2}$$

where $p(A_1)$ and $p(A_2)$ are each Rayleigh densities, as in (6.1).

In part I, it was shown how the assumptions of §2 above enable one to determine the probability density $p(S/A)$ for the steepness s of the short waves at the crest of a long wave of given amplitude A_1. Given s on A_1, and given the amplitude A_2 of the next wave, we can now integrate forwards using equation (2.6) to find the value of $s(\theta)$ at all points between the two wave crests. In this way we can determine the statistics of $s(\theta)$ over the complete surface profile.

As a check, this numerical procedures was first carried out in the limiting case $\kappa = 1$, corresponding to $A_2 = A_1$, and it was verified that the calculated values of $\overline{s^2}$, ϕ_0, $C_{\max}$ and $C(0)$ agreed with those found by the uniform (i.e. slowly varying) model in §6.

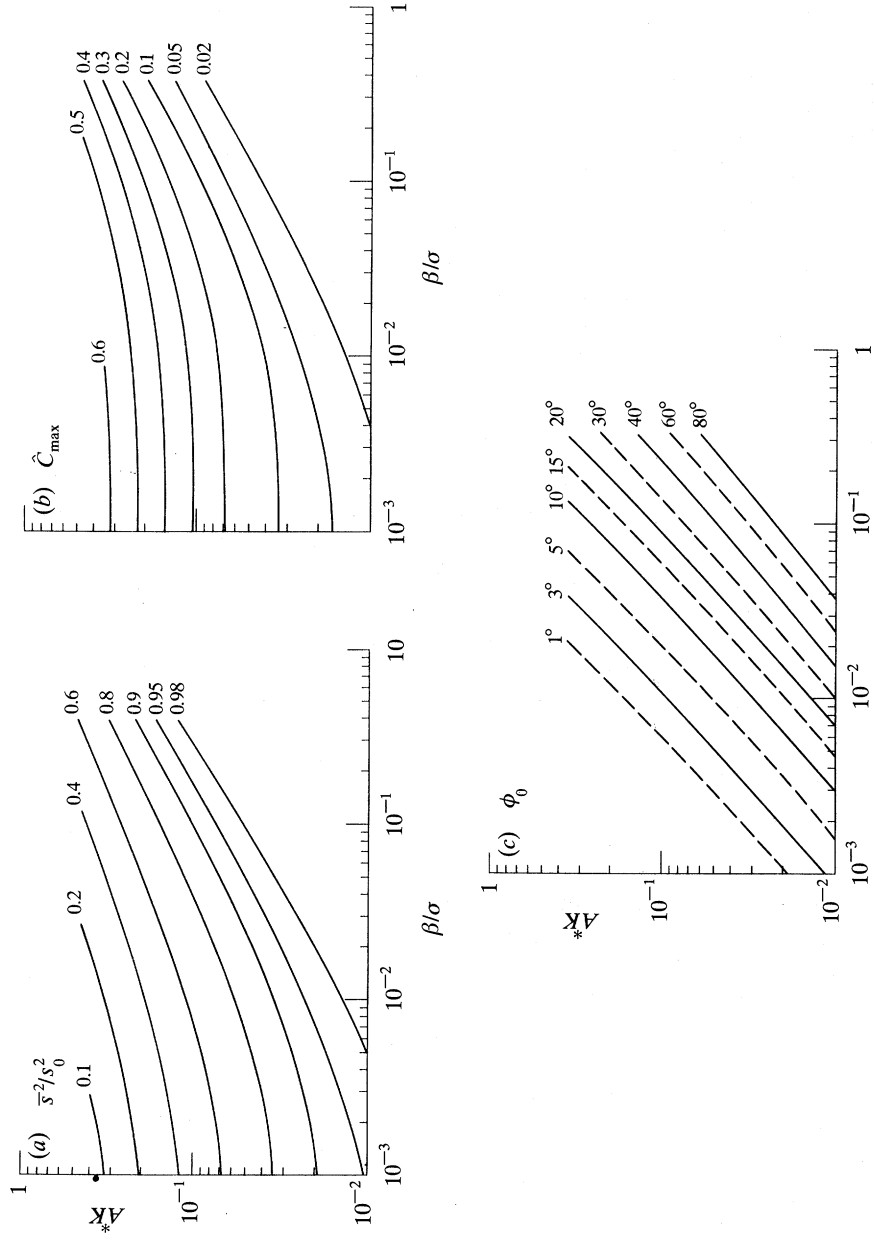

Figure 6. As figure 4, but with a bivariate density for successive long waves. $\kappa = 0$.

For general values of κ, when the amplitudes A_1 and A_2 are unequal, the calculation of $C(s^2, \eta)$ requires that we define the elevation η over the interval $0 < \theta < 4\pi$. We assumed that the amplitude varied 'piecewise linearly', that is

$$\eta = \begin{cases} [A_1 + (A_2 - A_1)\,\theta]\cos\theta, & 0 < \theta < 2\pi, \\ [A_2 + (A_3 - A_2)\,(\theta - 2\pi)]\cos\theta, & 2\pi < \theta < 4\pi, \end{cases}$$

where A_3 denotes the wave amplitude following A_2. To take full account of the variability of A_3 would be impractical computationally, but in the case $\kappa = 0$ we can reasonably replace A_3 by its constant mean value $\langle A \rangle = A^*$.

The results when $\kappa = 0$ are shown in figure 6*a–d*. Again it will be seen that the contours of $\overline{s^2}/s_0^2$, ϕ, $C_{\max}$ and C_0 are qualitatively similar to those in figure 4.

8. Comparison with observation

The strong effect of long-period waves in reducing the amplitude of short surface waves seems to have been first measured in the laboratory by Mitsuyasu (1966); see Phillips & Banner (1974). These authors generated long waves mechanically with a paddle wave maker, in a wind-wave flume. The quantity measured and tabulated by Phillips & Banner was the proportional reduction (r^2) in the mean-square elevation of the short wind-waves, as a function of the long-wave steepness AK. On the other hand the ratio $\overline{s^2}/s_0^2$ in the present theory refers to the relative mean-square steepness of the short waves. The slope spectrum of wind-waves being rather broad, these two quantities are not identical. Nevertheless one would expect them to behave in a qualitatively similar way. In fact, figures 7 and 8 of Phillips & Banner (1974) shows r^2 decreasing monotonically with AK from 1 at $AK = 0$ to about 0.35 at $AK = 0.1$. This is similar to the proportional reduction in $\overline{s^2}/s_0^2$ in figure 4 above, but about twice as great. Phillips & Banner (1974) attribute their observations and those of Mitsuyasu (1966) to the presence of a surface 'wind-drift' current, which we have neglected. The effectiveness of the wind-drift current in this respect has been questioned by Plant & Wright (1977).

Similar reductions in the spectral density of the surface elevation have also been measured in the laboratory by Donelan (1987). He finds that the reduction is greatest near the peak of the wind-wave spectrum, and becomes relatively small at higher frequencies, for a given value of AK. This again is in qualitative agreement with figure 4*a*. In his figure 6, for example, where $AK = 0.105$, the peak frequency at a distance $\Omega = 55$ m from the wave maker is 1.4 Hz. The corresponding growth rate, according to his observations, was $\beta = \frac{1}{2}\zeta = 0.0012\ \mathrm{s}^{-1}$. Hence β/σ, in figure 3*a* above, would be 0.00037. According to figure 3 above the value of s^2/s_0^2 at $AK = 0.105$ is 0.72. In figure 6 of Donelan (1987) the reduction lies between 0.20 at the peak frequency $f = f_{\mathrm{p}}$, and 1 at $f = f_{\mathrm{p}} \pm 0.5$ Hz.

Direct measurements of the slope spectrum have been made recently by Miller & Shemdin (1991; see also Miller *et al.* 1991). In these data the basic long-wave steepness was fixed at $AK = 0.041$ and the wind-speed varied from 4.0 to 10.0 m s^{-1} (one measurement at 1.5 m s^{-1} was rejected). The relevant parameters are given in table 1. Here s_1^2 is the measured mean-square surface slope in the absence of a mechanically generated long wave ($AK = 0$) and $\overline{s^2}$ is the same quantity with the long wave added. The next column shows the ratio of these two; it is always less than 1.

Table 1. *Parameters for the experiments of Miller et al. (1991)*

$W/(\mathrm{m\ s^{-1}})$	s_1^2	$\overline{s^2}$	$\overline{s^2}/s_1^2$	f_p/Hz	$\beta/\mathrm{s^{-1}}$	β/σ	s^2/s_0^2 (theory)
4.0	0.038	0.022	0.68	3.0	0.039	0.012	0.90
6.5	0.056	0.045	0.80	2.5	0.075	0.024	0.92
9.0	0.063	0.055	0.87	2.0	0.079	0.025	0.93
10.0	0.063	0.059	0.94	2.0	0.079	0.025	0.93

Table 2. *Amplitude and slope of the Fourier harmonics of the mechanically generated wave*

n	A_n	A_nK_n
1	4.11	0.043
2	0.40	0.015
3	0.46	0.038
4	0.04	0.013
5	0.01	0.008
6	0.02	0.003

The next columns of table 1 show f_p, the peak frequency of the slope spectrum and β, the growth-rate of the wind-generated waves, as calculated from Donelan's (1987) formula

$$\beta = 2.05\times10^{-5}(U_{L/2}/c-1)^{2.43}\,\omega. \tag{8.1}$$

Here $U_{L/2}$ denotes the wind-speed at a height of half a wavelength above the waves. We equate this to W. We also set $\omega = 2\pi f_\mathrm{p}$ and $c = g/\omega$. If we equate s_1 to s_0, then we may compare the fourth and the last columns of table 1. The agreement is closer at the higher wind-speeds, presumably because the short waves are closer to equilibrium with the wind and the underlying long waves, as assumed in the theory.

It has, however, been noted by Miller *et al.* (1991) that the mechanically generalized waves contained higher harmonics which, while contributing negligibly to the surface elevation, nevertheless produced significant components of the surface slope. This is shown in table 2, where the amplitudes A_n of the various harmonics are given. The harmonic $n = 3$, for example has an amplitude A_3 which is only one-tenth of the fundamental A_1. But because the frequency σ_n is proportional to n, the wavenumber K_n is proportional to n^2. Hence A_3K_3 is comparable in magnitude to A_1K_1. The ratio β/σ_n, however, is proportional only to n, and so varies less dramatically.

In this paper the wavenumber K of the long waves has been assumed to be constant, or nearly so. To take full account of the higher harmonics would require development of the theory beyond our present limits. However figure 3 suggests that if the values of AK and β/σ for the third harmonic were used instead of those for the first harmonic, then $\overline{s^2}/s_0^2$ would be somewhat less than the values given in table 1. Presumably the effect of both the first and third harmonics acting together is to reduce $\overline{s^2}/s_0^2$ still further, bringing it closer to the observed value of $\overline{s^2}/s_1^2$.

It should be emphasized that in these experiments the higher harmonics in the waveform were practically invisible to the naked eye, yet their effects on the mean-square slope $\overline{s^2}(\theta)$ were quite marked (see Miller *et al.* 1991). Similar effects may have been present in the previous experiments mentioned above.

Table 3. *Comparison of theoretical and observed values of* $\overline{s^2}/s_0^2$ *for the Pierson–Moskowitz spectrum*

$W/(\mathrm{m\ s^{-1}})$	β/σ_p	$\overline{s^2}/s_0^2$	$\overline{s^2} = s_H^2 + s_L^2$	$\overline{s^2}$ (obs)
6	0.100	0.906	0.051	0.030
8	0.154	0.949	0.053	0.041
10	0.215	0.976	0.054	0.051
12	0.282	0.993	0.055	0.061
14	0.356	0.998	0.056	0.071

9. Field observations

We have seen that the orbital contraction of the long waves is measured not by the long-wave amplitude A alone, but by the long-wave steepness AK. Thus the requisite information for the long waves is not the surface elevation spectrum $E(\sigma)$ which is usually measured, but the slope spectrum

$$S(\sigma) = k^2 E(\sigma), \quad k^2 = \sigma^2/g. \tag{9.1}$$

Often a low-frequency, or swell, component which is visible in the elevation spectrum $E(\sigma)$ may not be significantly present in the slope spectrum $S(\sigma)$.

Commonly used expressions for $E(\sigma)$ such as proposed by Pierson & Moskowitz (1964) are valid only at frequencies below about 0.5 Hz, and tend to underestimate the spectral density at higher frequencies. Direct measaurements of the slope spectrum are rare. Those by Shemdin & Hwang (1988) show a single broad peak, with a high-frequency behaviour like $f^{-1.5}$ approximately.

Field observations of sea surface slopes are known to be strongly influenced by other parameters such as atmospheric instability, as measured by the air–sea temperature difference (Hwang & Shemdin 1988). In fact, after removal of the temperature instability effect from the available data the residuals show a large scatter and no obvious dependence on the steepness of the dominant waves. (The value of A used seems to have been calculated from the significant wave height, not the mean wave height.) It is also unclear whether the 'significant waves' tabulated for example by Cox & Munk (1954) and used in this dataset were sufficiently separated from the short, steep waves to be counted as swell in the sense of the present paper.

10. Discussion

The present simplified model of long-wave/short-wave interaction, while including the features listed in §1, has neglected others that may be significant in some circumstances; particularly the wind-drift surface current discussed by Phillips & Banner (1974) and the weak nonlinear interactions between the short waves (Valenzuela & Laing 1972). The importance of the latter relative to the wind-generated growth rate has been discussed by Miller *et al.* (1991), in relation to the laboratory experiments described there. The two growth rates were shown to be of comparable magnitude. It is, however, arguable that the empirical formulae for the growth-rate derived by Plant (1982) or Donelan (1987), which we have used, do in fact include the short-wave interactions, so that these are already accounted for, though roughly.

A further deficiency of the model is the use of a single frequency to characterize the short-wave spectrum; especially since the growth-rate due to the wind depends

strongly on the short-wave frequency. However, it does appear from figures 3–5 that provided β/σ is less than 10^{-2}, both $\overline{s^2}/s_0^2$ and $C^*_{\max}$ and C^*_0 depend much more strongly on the long-wave steepness AK than on β/σ. Hence the dependence on short-wave frequency is not as critical as first appears.

Perhaps the most serious limitation of the model is that it applies strictly only in cases when there is a clear separation between the long waves (swell) and the shorter wind-waves in the slope spectrum. Such a separation can certainly be achieved in the laboratory. In the ocean, well-documented cases of such spectra in neutrally stable temperature conditions are still rare.

An alternative way to apply the theory, which suppresses the assumption of separation, is given in the Appendix. In this we consider simply an equilibrium wind-wave spectrum with a single peak frequency σ_p. The low-frequency part of the spectrum is assumed to be given by the Pierson & Moskowitz (1964) formula. The high-frequency part follows the laser observations of Shemdin & Hwang (1988). The latter is approximated by a single band of frequencies at the mean frequency of the higher band. The low-frequency part of the spectrum makes a small but constant contribution s_L^2 to the mean-square slope. The high-frequency contribution s_H^2 is obtained from figure 6*a* above, with the assumption that $s_0^2 = 0.0484$. Whereas s_L^2 is found to be a constant independent of the wind-speed, s_H^2 increases with W on account of the increase in $\overline{s^2}/s_0^2$ with β/σ in figure 6*a*. The sum $(s_L^2 + s_H^2)$ is compared with Cox & Munk's empirical formula for the total mean squared slope in table 3. It will be seen that there is agreement between theory and observation at about $W = 10$ m s^{-1}. Also, the rate of increase in $(s_L^2 + s_H^2)$ with W is of the correct sign but too low in absolute value. No doubt the reason is that much of the observed increase in mean-square slopes with increasing wind-speed is due to the broadening of the slope spectrum due to the progressive lowering of the low-frequency cut-off. The highest frequencies in the spectrum are affected less by the 'swell' than by the short waves of intermediate frequency on which they ride; it is only the intermediate waves which are reduced by the 'swell'.

Indeed, in a broad spectrum of wind-waves we may expect that reduction of the energy in the peak frequencies by interaction which swell waves will lead to an increase of energy in the highest frequencies. Evidence of this effect can be clearly seen in the spectra recorded by Donelan (1974). To represent the phenomenon satisfactorily an n-scale model is required, with $n > 2$.

The calculations in §5 were begun while the author was visiting the California Institute of Technology Jet Propulsion Laboratory in 1987. The author thanks particularly Victor Zlotnicki for technical assistance and Omar Shemdin for general discussions. The completion of the work was made possible by the Office of Naval Research under Contract N00014-86-C-0303 to Ocean Research and Engineering, Pasadena, California, U.S.A.

Appendix. Application to an equilibrium wind-wave spectrum

Consider the surface-elevation spectrum $E(\sigma)$ proposed by Pierson & Moskowitz (1964) for winds between 0 and 10 m s^{-1}, namely

$$E(\sigma) = \alpha g^2 \sigma^{-5} \mathrm{e}^{-\beta(\sigma_0/\sigma)^4}, \tag{A 1}$$

where $\alpha = 0.0081$, $\beta = 0.74$ and

$$\sigma_0 = g/W, \tag{A 2}$$

W being the wind-speed. This has a maximum when

$$\sigma/\sigma_0 = [4\beta/5]^{\frac{1}{4}} = 0.877. \tag{A 3}$$

The slope spectrum corresponding to (A 1) is

$$S_L(\sigma) = \alpha\sigma^{-1}\,\mathrm{e}^{-\beta(\sigma_0/\sigma)^4}, \tag{A 4}$$

which has a maximum when

$$\sigma/\sigma_0 = (4\beta)^{\frac{1}{4}} = 1.312, \tag{A 5}$$

differing from (A 3) by a factor 1.5, approximately. We shall denote the frequency corresponding to (A 5) by σ_p, so

$$\sigma_\mathrm{p} = 1.312g/W. \tag{A 6}$$

Suppose that equation (A 4) adequately represent the low-frequency part of the spectrum, that is in the range

$$0 < \sigma < \sigma_1, \quad \sigma_1 = n\sigma_\mathrm{p}, \tag{A 7}$$

where n is a factor of order 2. Then in the two-scale model it is reasonable to assume that the long wave has a mean steepness A^*K given by

$$(A^*K)^2 = \tfrac{1}{4}\pi\,\langle(AK)^2\rangle = \tfrac{1}{2}\pi\,\overline{s_L^2}, \tag{A 8}$$

where

$$\overline{s_L^2} = \int_0^{\sigma_1} s_L(\sigma)\,\mathrm{d}\sigma. \tag{A 9}$$

On substituting from (A 4) and changing the variable of integration to $x = \beta(\sigma_0/\sigma_1)^4$ we obtain

$$\overline{s_L^2} = \tfrac{1}{4}\alpha \int_{\frac{1}{4}n^4}^{\infty} \frac{\mathrm{e}^{-x}}{x}\,\mathrm{d}x. \tag{A 10}$$

When $n = 2$, for example, this gives

$$\overline{s_L^2} = 0.007\,28, \tag{A 11}$$

hence

$$A^*K = 0.107 \tag{A 12}$$

by (A 8). We assign to the long waves the peak spectral frequency σ_p given by equation (A 6).

Consider now the high-frequency part of the spectrum. The laser observations by Shemdin & Hwang (1988) at wind-speeds between 2.8 and 6.2 m s^{-1} show that over the range 1 Hz $< f <$ 16 Hz the slope spectrum falls off roughly like $f^{-1.5}$, that is slightly more steeply than in (A 4). Above 16 kHz the fall-off is again steeper. Notice that any spectrum of the form $S \propto \sigma^{-1.5}$ over a range $\sigma_1 < \sigma < \sigma_2$ has a mean frequency

$$\int_{\sigma_1}^{\sigma_2} \sigma S\,\mathrm{d}\sigma \Big/ \int_{\sigma_1}^{\sigma_2} S\,\mathrm{d}\sigma = (\sigma_1\sigma_2)^{\frac{1}{2}}. \tag{A 13}$$

Thus we shall assign to the short waves in the model a mean frequency

$$\omega = (n\sigma_\mathrm{p}\,\sigma_\mathrm{q})^{\frac{1}{2}}, \tag{A 14}$$

where σ_p is the peak frequency (A 6) and σ_q is a cut-off frequency: $2\pi \times 16$ rad s^{-1}.

For the rate of growth β of the short waves we adopt Plant's (1982) formula

$$\beta = 0.04\,(u_*/c)^2\,\omega\cos\theta, \tag{A 15}$$

where u_* is the wind friction velocity, c the phase speed and θ the angle between the wind and the wave velocity. Taking $u_* = 0.04W$, $c = g/\omega$ and $\theta = 0$ this yields

$$\beta = 0.64\times10^{-4}\,(W/g)^2\,\omega^3. \tag{A 16}$$

From this and (A 12) we have

$$\begin{aligned}\beta/\sigma_{\mathrm{p}} &= 0.73\times10^{-4}\,(n\sigma_{\mathrm{q}}\,W/g)^{\frac{3}{2}}\\ &= 0.0024(nW)^{\frac{3}{2}}\end{aligned} \tag{A 17}$$

if W is measured in m s^{-1}

Suppose first that $n = 2$. Then knowing the two parameters A^*K and $\beta/\omega_{\mathrm{p}}$ given by (A 12) and (A 16) we may enter figure 6*a*, for example, to find $\overline{s_H^2}$, the mean-square slope of the short waves. To this we must add s_L^2 given by (A 11) to obtain the total mean-square slope

$$s^2 = \overline{s_L^2} + \overline{s_H^2}. \tag{A 18}$$

In table 3 the results are evaluated at various wind-speeds W and are compared with the empirical formula

$$s^2 = 5.12\times10^{-5}\,W \tag{A 19}$$

given by Cox & Munk (1954), from sun glitter measurements.

References

Cox, C. S. & Munk, W. H. 1954 Statistics of the sea surface derived from sun glitter. *J. Mar. Res.* **13**, 198–227.

Donelan, M. A. 1987 The effect of swell on the growth of wind waves. *Johns Hopkins Univ. APL Tech. Dig.* **8**, 18–23.

Hwang, P. A. & Shemdin, O. H. 1988 The dependence of sea surface slope on atmospheric stability and swell conditions. *J. geophys. Res.* **93**, 13903–13912.

Jähne, B. 1989 Energy balance in small-scale waves – an experimental approach using optical slope measuring technique and image processing. In *Radar scattering from modulated wind-waves* (ed. G. J. Komen & W. A. Oost), pp. 105–120. Dordrecht: Kluwer.

Longuet-Higgins, M. S. 1980 On the distribution of the heights of sea waves: some effects of nonlinearity and finite band width. *J. geophys. Res.* **85**, 1519–1523.

Longuet-Higgins, M. S. 1987 A stochastic model of sea surface roughness. I. Wave crests. *Proc. R. Soc. Lond.* A **410**, 19–34.

Miller, S. J. & Shemdin, O. H. 1991 Measurement of the hydrodynamic modulation of centimeter waves. *J. geophys. Res.* **96**, 2749–2759.

Miller, S. J., Shemdin, O. H. & Longuet-Higgins, M. S. 1991 Laboratory measurements of modulation of short wave slopes by long surface waves. *J. Fluid Mech.* (In the press.)

Mitsuyasu, H. 1966 Interactions between water waves and wind. I. *Rep. Res. Inst. Appl. Mech. Kyushu Univ.* **14**, 67–88.

Phillips, O. M. & Banner, M. L. 1974 Wave breaking in the presence of wind drift and swell. *J. Fluid Mech.* **66**, 625–640.

Pierson, W. J. & Moskowitz, L. 1964 A proposed spectral form for fully developed wind seas based on the similarity theory of S. A. Kitaigorodskii. *J. geophys. Res.* **69**, 5181–5190.

Plant, W. J. & Wright, J. W. 1977 Growth and equilibrium of short gravity waves in a wind-wave tank. *J. Fluid Mech.* **82**, 767–793.

Plant, W. J. 1982 A relationship between wind stress and wave slope. *J. geophys. Res.* **87**, 1961–1967.

Shemdin, O. H. & Hwang, P. A. 1988 Comparison of measured and predicted sea surface spectra of short waves. *J. geophys. Res.* **93**, 13883–13890.

Valenzuela, G. R. & Laing, M. B. 1972 Nonlinear energy transfer in a gravity-capillary wave spectrum, with applications. *J. Fluid Mech.* **54**, 507.520.

Wenz, F. J. 1976 Cox and Munk's sea surface slope variance. *J. geophys. Res.* **81**, 1607–1608.

Received 20 February 1991; accepted 25 March 1991